

# UC Berkeley

## UC Berkeley Previously Published Works

### Title

Nonmetal-to-Metal Transition of Magnesia Supported Au Clusters Affects the Ultrafast Dissociation Dynamics of Adsorbed CH<sub>3</sub>Br Molecules

### Permalink

<https://escholarship.org/uc/item/9kp1d382>

### Journal

The Journal of Physical Chemistry Letters, 13(21)

### ISSN

1948-7185

### Authors

Vaida, Mihai E  
Rawal, Takat B  
Bernhardt, Thorsten M  
[et al.](#)

### Publication Date

2022-06-02

### DOI

10.1021/acs.jpcllett.2c00968

### Copyright Information

This work is made available under the terms of a Creative Commons Attribution-NonCommercial License, available at <https://creativecommons.org/licenses/by-nc/4.0/>

Peer reviewed

# Non-metal to metal transition of magnesia supported Au clusters affects the ultrafast dissociation dynamics of adsorbed CH<sub>3</sub>Br molecules

*Mihai E. Vaida<sup>1,2\*</sup>, Takat B. Rawal<sup>1</sup>, Thorsten M. Bernhardt,<sup>3\*</sup> Brett M. Marsh,<sup>4</sup>  
Talat S. Rahman,<sup>1,2</sup> Stephen R. Leone<sup>4,5,6\*</sup>*

<sup>1</sup>Department of Physics, University of Central Florida, Orlando, Florida 32816, United States

<sup>2</sup>Renewable Energy and Chemical Transformations Cluster, University of Central Florida, Orlando, Florida 32816, United States

<sup>3</sup>Institute of Surface Chemistry and Catalysis, University of Ulm, 89069 Ulm, Germany

<sup>4</sup>Department of Chemistry, University of California, Berkeley, California 94720, United States

<sup>5</sup>Department of Physics, University of California, Berkeley, California 94720, United States

<sup>6</sup>Chemical Sciences Division, Lawrence Berkeley National Laboratory, Berkeley, California 94720, United States

## Abstract:

The detection of intermediate species and the correlation of their ultrafast dynamics with the morphology and electronic structure of a surface is crucial to fully understand and control heterogeneous photoinduced and photocatalytic reactions. In this work, the ultrafast photodissociation dynamics of CH<sub>3</sub>Br molecules adsorbed on variable size Au clusters on MgO/Mo(100) is investigated by monitoring the CH<sub>3</sub><sup>+</sup> transient evolution using a pump-probe technique in conjunction with surface mass spectrometry. Furthermore, extreme-ultraviolet photoemission spectroscopy in combination with theoretical calculations are employed to study the electronic structure of the Au cluster on MgO/Mo(100). Changes in the ultrafast dynamics of CH<sub>3</sub><sup>+</sup> fragment are correlated with the electronic structure of Au as it evolves from monomers to small nonmetallic clusters to larger nanoparticles with a metallic character. This work provides a new avenue to a detailed understanding of how surface photoinduced chemical reactions are influenced by the composition and electronic structure of the surface.

---

\*) Authors to whom correspondence should be addressed. E-mail: [mihai.vaida@ucf.edu](mailto:mihai.vaida@ucf.edu), Tel: +1 407-823-4213, E-mail: [thorsten.bernhardt@uni-ulm.de](mailto:thorsten.bernhardt@uni-ulm.de), Tel: +49 731-50-25455, and E-mail: [srl@berkeley.edu](mailto:srl@berkeley.edu), Tel: +1 510-643-5467

Gold clusters and nanoparticles have sparked intense interest over the years because of their size dependent electronic, optical, and chemical properties,<sup>1-2</sup>(and ref. therein) with applications in sensors,<sup>3</sup> probes,<sup>4</sup> biological systems and medicine,<sup>5-7</sup> as well as energy conversion, which includes solar cells,<sup>8-10</sup> catalysis,<sup>11-13</sup> (and ref. therein) and photocatalysis.<sup>14</sup> Not surprisingly, theoretical and experimental studies of small clusters have been performed to investigate their electronic<sup>15-19</sup> and geometric structure,<sup>17, 20-32</sup> as well as their catalytic properties,<sup>11</sup> with a vast amount of investigations focusing on the CO oxidation reaction.<sup>19, 33-38</sup> Large gold nanoparticles were often studied and employed in various applications because of their optical properties as facilitated by the localized surface plasmon resonance effect.<sup>3, 7-8, 14, 39</sup>

Despite the large number of experimental and theoretical investigations that explored properties of free and supported gold nanoparticles, which have led to various scientific breakthroughs and technological applications,<sup>3, 39-40</sup> there is a lack of knowledge on how small gold clusters that do not present localized surface plasmon resonances could influence photoinduced chemical reactions at surfaces. With the above in mind, the present investigation explores photoinduced chemical reactions on oxide surfaces decorated with gold clusters, in the size range close to the nonmetal-to-metal transition.

To investigate the molecular photodissociation dynamics of the CH<sub>3</sub>Br molecules on magnesia supported gold clusters, a technique is employed that combines femtosecond (fs) laser pump–probe spectroscopy with multiphoton ionization and time-of-flight mass spectrometry.<sup>41</sup> The technique relies on the dissociation of the adsorbed CH<sub>3</sub>Br molecules via two-photon pump excitation of the A-band followed by three-photon probe resonance multiphoton ionization at the surface to detect the CH<sub>3</sub> fragments by mass spectrometry of the desorbed ions.<sup>42</sup> The center wavelength of the pump and probe laser beams are 266 nm and 333 nm, respectively. Details about the experimental setups and the pump-probe technique used in this investigation are presented in the Supplementary Information (see section 1 and 2 in the Supplementary Information).

Figure 1 displays a series of transient signals monitoring the photodissociation dynamics of CH<sub>3</sub>Br dosed on the surface at 100 K temperature by detecting the emerging methyl cation signal as a function of the pump-probe time delay. The transients are recorded from MgO surfaces prepared with different amounts of gold between 0.065 monolayer equivalent (ML) and 0.15 ML. For reference, in each case a CH<sub>3</sub><sup>+</sup> transient was recorded from the bare magnesia surface just

before gold deposition (blue circles in Figure 1). The methyl bromide coverage, which is 0.25 ML, and the laser parameters are kept constant for all recorded transient signals.

On the bare magnesia thin film, the transient methyl signal starts with an initial delay of  $150 \pm 50$  fs and exhibits a single exponential rise with a time constant of  $320 \pm 60$  fs, which are in a perfect agreement with the previous  $\text{CH}_3\text{Br}$  photodissociation measurements on MgO thin films.<sup>43-46</sup> The initial coherent delay of  $150 \pm 50$  fs reflects the minimal time needed for the liberation of the methyl fragments from the molecular force field and from the force field of the magnesia surface. This time is longer than the A-band dissociation time of  $\text{CH}_3\text{Br}$  in the gas phase, i.e.  $116 \pm 25$  fs,<sup>47</sup> due to the molecular adsorption geometry in which the C–Br axis is almost parallel to the MgO substrate, which facilitates collision of the  $\text{CH}_3$  fragment with the adjacent molecule just before being released into gas phase.<sup>(45 and refs. therein)</sup> The subsequent growth of the methyl signal with a time constant of  $320 \pm 60$  fs, which is obtained from data fitting with a ‘delayed exponential rise’ function convoluted with the pump-probe cross correlation function<sup>48</sup> (red curve in Figure 1a) is attributed to the average lifetime of all trajectories leading to the release of the methyl fragment.

The transient methyl signal obtained from the photodissociation of  $\text{CH}_3\text{Br}$  (dosed at 100 K) on magnesia covered by 0.065 ML Au, deposited previously at 100 K, displayed in Figure 1a (black squares) is essentially similar to the one obtained from the bare MgO surface (Figure 1a - blue circles). After deposition of 0.1 ML Au on the magnesia surface, the transient methyl signal, which is displayed in Figure 1b, also exhibits an exponential rise, but in addition it displays a new peaked structure with a maximum at 240 fs. Fitting the experimental data with a model that consists of an exponential ‘rise and decay’ in conjunction with a ‘delayed exponential rise’, convoluted with the laser cross correlation<sup>48</sup> (red curve in Figure 1b) gives  $190 \pm 30$  fs for the rise and decay of the peaked structure, attributed below to gold particles on the surface. For the subsequent exponential rise at longer delay times, the time constant matches with the one obtained from the bare MgO surface.

Figure 1c shows the transient methyl signal obtained from the photodissociation of  $\text{CH}_3\text{Br}$  on magnesia covered by 0.13 ML Au. In this transient signal, the peaked structure at early delay times with a maximum intensity at 270 fs is even more apparent and is followed by an exponential rise. The best fit with the same model as in Figure 1b to the experimental data (Figure 1c - black squares) gives similar time constants of  $200 \pm 30$  fs for the rise and the decay components of the

observed peaked structure in time. For the subsequent exponential rise at longer delay times, the time constant matches again with the one obtained from bare MgO surface. The  $\text{CH}_3^+$  transient peaked structure observed in Figure 1 b,c appears only on magnesia substrates prepared with gold particles (coverages between 0.1 and less than 0.15 ML). The photodissociation of  $\text{CH}_3\text{Br}$  on MgO/Mo(100) covered by 0.15 ML Au leads to a dramatic increase of the methyl cation signal intensity (factor of six) compared to the signal obtained from the bare magnesia surface (cf. Figure 1d). However, no time dependence of the  $\text{CH}_3^+$  signal is observed any more. These new features are all assigned to the dissociation of methyl bromide molecules adsorbed on the gold clusters.

For the interpretation of the transient data in Figure 1(b-d), the size dependent structure of the gold clusters on MgO is considered, which was previously investigated via scanning tunneling microscopy (STM) and electron paramagnetic resonance (EPR) spectroscopy by Freund and coworkers.<sup>49-50</sup> According to the STM and EPR investigations, at low gold coverages up to 0.06 ML on 8 ML MgO/Mo(100), at 100 K, mostly gold atoms are observed on the surface. Consequently, it can be assumed that in the present investigation, isolated gold atoms and very small clusters are present on the MgO surfaces for an Au coverage of 0.065 ML (cf. Figure 1a), and these do not lead to a  $\text{CH}_3^+$  transient peaked structure. This conclusion is further supported by an experiment in which Au atoms produced by a mass-selected cluster source, coupled to the investigation chamber, were soft landed on 10 ML MgO/Mo(100) surface (Au coverage of about 0.03 ML). In this experiment, no  $\text{CH}_3^+$  transient peaked structure is observed (not shown here). Furthermore, Popolan et al,<sup>51</sup> demonstrated that isolated, small gold clusters, i.e.  $\text{Au}_1$ - $\text{Au}_3$ ,  $\text{Au}_5$ , and  $\text{Au}_7$ , interact strongly with  $\text{CH}_3\text{Br}$ , break the C-Br bond and subsequently liberate the  $\text{CH}_3$  radicals, while the Br atoms remain attached to the clusters. Therefore, it is assumed that very small gold clusters, produced by evaporation of 0.065 ML Au on MgO at 90 K, dissociate the  $\text{CH}_3\text{Br}$  molecules directly and trap the Br atoms. Consequently, the  $\text{CH}_3^+$  transient pump-probe laser signal in Figure 1a originates just from  $\text{CH}_3\text{Br}$  molecules adsorbed on the MgO surface and not from  $\text{CH}_3\text{Br}$  adsorbed on small Au clusters on MgO.

Small Au clusters are expected to form on the magnesia surface, as the Au coverage is increased above 0.065 ML. Apparently, in contrast to magnesia supported Au atoms, the  $\text{CH}_3\text{Br}$  photodissociation on small Au clusters on MgO/Mo(100) leads to the appearance of the  $\text{CH}_3^+$  transient peaked structure in the laser pump-probe experiment, as shown in Figure 1b,c. The

dramatic increase of the methyl cation signal intensity detected from the magnesia surface when covered by 0.15 ML Au (Figure 1d) is attributed to the photodissociation on larger Au particles, which might have electronic properties different from the Au particles obtained at lower coverages.

STM investigations of Freund and coworkers demonstrate that large three dimensional Au particles are formed via sintering, if MgO samples decorated with gold atoms (Au coverages below 0.06 ML) are annealed to 300 K.<sup>49</sup> Therefore, in order to confirm the hypothesis that large particles are responsible for the change of the methyl signal at coverages above 0.15 ML Au (Figure 1d), the magnesia sample with 0.13 ML Au (Figure 1c) was briefly heated to 800 K to induce the formation of larger Au particles via sintering. Subsequently, CH<sub>3</sub>Br molecules are dosed on the surface at 100 K, and a CH<sub>3</sub><sup>+</sup> transient signal is recorded. The result is displayed in the inset of Figure 1c. Indeed, the peak structure and exponential rise measured before the annealing (Figure 1c) are not observed anymore. Instead, an intense methyl signal is obtained that does not exhibit a time dependence, similar to the case of 0.15 ML coverage in Figure 1d. This result supports the hypothesis that the presence of a considerable fraction of large Au nanoparticles are responsible for the different signal in Figure 1d.

By reducing the intensity of both pump and probe laser pulses by a factor of three, a time dependent measurement of CH<sub>3</sub>Br photodissociation on the surface decorated with large Au particles is possible. Figure S2 in the Supplementary Information displays the CH<sub>3</sub><sup>+</sup> transient signal recorded with reduced pump and probe beam laser intensities from a MgO/Mo(100) surface covered by 0.13 ML Au and annealed to 800 K. The CH<sub>3</sub><sup>+</sup> transient signal presents a broad peak (1.1 ps at the FWHM) structure with a maximum located at about 450 fs. Due to the high noise level, only a Gaussian function (solid line in Figure S2) is drawn to guide the eye. The reduced laser intensity used to record the CH<sub>3</sub><sup>+</sup> transient signal and the shape of this transient signal further indicates a similar excitation and detection mechanism as for CH<sub>3</sub>Br adsorbed on an extended Au surface.<sup>42</sup> As mentioned above, two photons at 266 nm are necessary to induce the CH<sub>3</sub>Br photodissociation on a 10 ML MgO/Mo(100) surface, while three photons at 333.3 nm are necessary to detect the CH<sub>3</sub> fragments through (2+1) REMPI.<sup>43</sup> On an extended Au surface, power dependence measurements reveal that a single pump photon at 266 nm is absorbed, while the CH<sub>3</sub> ionization-detection is accomplished by two probe photons at 333.3 nm.<sup>43</sup> The reduced number of photons necessary for the photoexcitation of CH<sub>3</sub>Br and detection of CH<sub>3</sub><sup>+</sup> from an Au surface is attributed to a red-shift of the CH<sub>3</sub>Br A-band by about 1.5 eV,<sup>42</sup> as also observed for CH<sub>3</sub>Br

adsorbed on Ag(111).<sup>52</sup> The  $\text{CH}_3^+$  transient signal, i.e. peaked structure, recorded on the Au surface is attributed to the following pump-probe schema: (i) a single pump photon at 266 nm excites the  $\text{CH}_3\text{Br}$  molecule into the dissociative A-band; (ii) before the molecule dissociates, two-probe photons at 333 nm further excite the molecule from the A-band into a cationic dissociative state which decomposes and leads to the  $\text{CH}_3^+$  transient signal.<sup>42</sup> It is assumed that the  $\text{CH}_3^+$  transient peaked structure observed at about 240 fs and 270 fs in Figure 1 (b and c) has a similar excitation and detection mechanism as for  $\text{CH}_3\text{Br}$  on the extended Au surface; this indicates that non-metallic Au particles consisting of several atoms are also capable of perturbing the electronic structure of the  $\text{CH}_3\text{Br}$  molecules. Because of the low number of photons necessary to record the  $\text{CH}_3^+$  transient signals from extended Au surfaces and Au particles with a metallic character, only an intense, non-time dependent  $\text{CH}_3^+$  signal is observed in Figure 1d and insert in Figure 1c.

In order to correlate the ultrafast dissociation dynamics of the  $\text{CH}_3\text{Br}$  molecules with the electronic structure of the Au clusters on MgO/Mo(100) and also to understand the dramatic increase of the methyl cation signal observed in Figure 1d as the Au coverage exceeds 0.15 ML, the electronic structure of the Au/MgO/Mo(100) system is studied using static femtosecond extreme ultraviolet (XUV) photoemission spectroscopy.<sup>53-55</sup>

Figure 2(a) displays the photoemission spectra of the bare Mo(100) substrate, of 10 ML MgO grown on Mo(100), and photoemission spectra recorded from various amounts of Au, ranging from 0.01 ML to 1.00 ML, deposited on 10 ML MgO/Mo(100). The photoemission spectra are recorded using the 23<sup>rd</sup> harmonic (35.65 eV) of the Ti:Sapphire laser fundamental wavelength for photoexcitation. The binding energy in Figure 2 is referenced to the Fermi level ( $E_F = 0$ ), which is approximately at the center of the Fermi Dirac distribution of the Mo(100) substrate.<sup>53-54</sup> The photoemission onset of Mo(100) coincides with the photoemission onset of 0.15 ML- 1.00 ML Au/MgO/Mo(100), which is located at 0.08 eV above the Fermi level.

When 10 ML MgO are grown on Mo(100) the photoemission onset shifts to -3.4 eV below the  $E_F$  (larger negative numbers refer to greater binding energies), as determined by the intersection point where the extrapolation of the linear portion of the MgO rising edge intersects the straight line describing the background (see red dashed line in Figure 2a).<sup>55-56</sup> The occupied electronic states below -3.4 eV are attributed to the photoemission from the O-2p states that make up the valence band of MgO. No photoemission peaks are observed at binding energies between 0 eV

and -3.4 eV, which corresponds to the portion of the MgO band gap that can be accessed via photoemission spectroscopy, indicating that the MgO film is fully oxidized.

When gradually increasing amounts of Au are evaporated on the 10 ML MgO film, the photoemission progressively shifts to lower binding energy. The shift of the photoemission to lower binding energy as the amount of gold is increased (cf Figure 2(a)), is attributed to a lowering of the work function of the combined system, i.e. Au/MgO/Mo(100). This shift is expected to be due to the electrostatic interaction between the photoemitted electrons and the negative charges that accumulate at the cluster-oxide interface, which increases with the number of Au atoms in direct contact with the oxide surface.<sup>57</sup>

To explore the change in the electronic structure of the Au particles as their size is increased, and to eliminate the influence of the substrate, in Figure 2(b) the photoemission spectrum of the bare MgO/Mo(100) substrate is subtracted from the photoemission spectra of Au/MgO/Mo(100). Distinct photoemission features centered at -1.35 eV, -2.2 eV (cf. Figure 2(b)) and -3.30 eV (cf. Figure 2(a)) are observed. As the amount of Au on MgO/Mo(100) is varied, these features change their relative intensities but do not shift in energy (cf. Figure 2(b)). The highest intensity of the photoemission feature centered at -2.2 eV is observed for Au coverages of 0.02 ML, while the feature centered at -1.35 eV is most prominent for Au coverages of 0.06 ML to 0.12 ML. The photoemission feature at -2.20 eV fades out for Au coverages larger than 0.07 ML, while the -1.35 eV feature diminishes for coverages larger than 0.12 ML Au. The photoemission feature at -3.30 eV is visible only at high Au coverages, i.e. 0.38 ML and 1.00 ML. In addition, a low intensity photoemission feature centered at -0.75 eV is observed in Figure 2(b) for low Au coverages of 0.01-0.10 ML. Note that the photoemission features at -2.2 eV, -1.35 eV, and -0.75 eV discussed above are not present in the photoemission spectra of bare Mo(100) or 10 ML MgO/Mo(100).

The peak at -3.30 eV is attributed to the photoemission from large Au particles, since this peak is visible only at high Au coverages. The distinct features at -2.2 eV, -1.35 eV, and -0.75 eV are attributed to photoemission from Au atoms and clusters composed of very few atoms on MgO/Mo(100). Since the photoemission feature at -2.2 eV displays the highest intensity at Au coverages of 0.01-0.06 ML, the result suggests that this photoemission feature originates from Au atoms on MgO/Mo(100). This is in agreement with the STM and EPR investigations,<sup>49-50</sup> which reveal that mostly gold atoms are present on the MgO/Mo(100) surface decorated with Au

coverages lower than 0.06 ML. Moreover, theoretical investigations of Pacchioni and coworkers show that Au atoms on 3 ML of MgO(100) have the Au-5d density of states located between -1.5 eV and -2.5 eV, below the Fermi level.<sup>58</sup> In a different theoretical investigation, by Häkkinen and coworkers, it was shown that the Au atoms at hollow sites on 3 ML MgO/Mo(100) have the Au 5d electrons centered at -2 eV below the Fermi level.<sup>59</sup> Therefore, the feature at -2.2 eV in Figure 4(b) is attributed to the photoemission from Au-5d states belonging to Au atoms on MgO/Mo(100). The peak at -1.35 eV might be due to the Au-5d electrons of Au clusters composed of a few atoms, since this peak is visible between 0.06-0.12 ML Au and is barely visible at coverages below 0.06 ML Au. The low intensity feature at -0.75 eV is attributed to photoemission from the Au-6s states of Au atoms. This photoemission feature matches the predicted energetic position and relatively low intensity of the Au 6s electrons of Au atoms.<sup>58-59</sup> Furthermore, the photoemission feature initially centered at -0.75 eV systematically expands toward lower binding energies, as the amount of gold is increased above 0.1 ML, lowering the onset energy of the photoemission spectra.

For Au coverages up to 0.12 ML the photoemission onsets are located below the Fermi level, indicating that the Au clusters have a non-metallic character, while for a Au coverage of 0.15 ML, the photoemission onset shifts to +0.08 eV above the Fermi level, similar to the photoemission from metals. The photoemission onset does not change for Au coverages larger than 0.15 ML and coincides with the photoemission onset of the Mo(100) substrate. This clearly indicates that Au particles formed at Au coverages of 0.15 ML or greater have a metallic character. Consequently, the transition of Au clusters from nonmetal to metal on a 10 ML MgO film grown on Mo(100) occurs at Au coverages of about 0.15 ML.

The static fs-XUV photoemission data obtained from various amounts of Au on 10 ML MgO/Mo(100) (cf. Figure 2) strongly suggest that the dramatic increase in the  $\text{CH}_3^+$  signal observed when 0.15 ML Au is evaporated on the surface is due to the formation of Au particles that have a metallic character. The photodissociation mechanism of the  $\text{CH}_3\text{Br}$  molecule on metallic Au particles is expected to be broadly similar to the photodissociation mechanism on an extended Au surface,<sup>42</sup> due to the red-shift of the  $\text{CH}_3\text{Br}$  A-band by the metal structure, as discussed above. Certainly, the morphology of various Au particles that have a metallic character might also play a role in the photodissociation of  $\text{CH}_3\text{Br}$ , however, the changeover of Au from non-metal to metal plays the essential role.

To correlate the Au particle size with the photoemission experiments and ultimately with the changes observed in photodissociation dynamics as the Au loading on MgO/Mo is varied, density functional theory (DFT) investigations have been performed to estimate the size at which the Au clusters become metallic on the MgO support. Details about the DFT calculation as well as the calculated density of states (DOS) of gold clusters consisting of 13, 19, 43, 55, 79, and 135 atoms on MgO, with and without including the DOS of MgO are presented in the Supplementary Information (see Figures S1 and S3). The theoretical investigation reveals that no occupied electronic states are present in the vicinity of the Fermi level for Au<sub>13</sub>, Au<sub>19</sub> and Au<sub>47</sub>. However, for Au clusters containing 55 or more atoms, occupied electronic states are detected at the Fermi level (Figure S3), indicating that these clusters have a metallic character. Therefore, from the photoemission experiments (cf. Figure 2) and theoretical investigations (cf. Figure S3) we can conclude that the evaporation of 0.15 ML Au on MgO leads to the formation of Au clusters that have at least 55 atoms. These metallic Au clusters drastically influence the photodissociation dynamics of CH<sub>3</sub>Br due to the perturbation of the excited states of the molecule as explained above.

In summary, the ultrafast photodissociation dynamics of CH<sub>3</sub>Br molecules on magnesia films decorated with variable size Au clusters is investigated by monitoring the transient evolution of the CH<sub>3</sub><sup>+</sup> signal via pump-probe femtosecond-laser mass spectrometry technique. To correlate the CH<sub>3</sub>Br photodissociation dynamics with the electronic structure of the surface and the Au cluster size on the MgO/Mo(100) surface, fs-XUV photoemission experiments and DFT calculations have been performed.

No difference between the CH<sub>3</sub><sup>+</sup> transients obtained from bare MgO and MgO films decorated mostly with Au monomers (i.e. 0.065 ML Au/MgO/Mo(100)) is observed, because such small Au clusters composed of a few atoms break the CH<sub>3</sub>Br molecule bond, release the CH<sub>3</sub> fragment and trap the Br atom, as previously demonstrated.<sup>51</sup> For Au coverages of 0.15 ML, which coincides with the formation onset of Au particles that have a metallic character, a large increase in the CH<sub>3</sub><sup>+</sup> signal intensity and a loss of a time dependent signal is observed due to a change in the pump-probe mechanism. Reducing the intensity of both pump and probe laser beams by a factor of three, leads to a time dependent CH<sub>3</sub><sup>+</sup> signal that resembles the transient signal obtained from extended Au surfaces. DFT investigations show that the non-metal to metal transition of magnesia supported Au clusters occurs as the cluster size exceeds 55 atoms, providing an estimate

of the particle size at which the photodissociation dynamics of  $\text{CH}_3\text{Br}$  is drastically influenced by the Au clusters.

At intermediate Au coverages of 0.10 ML and 0.13 ML, clusters consisting of tens of atoms, i.e. sizes larger than a few atoms, but smaller than particles that have a metallic character ( $> 55$  atoms) are formed. The  $\text{CH}_3^+$  transient peak structure detected from 0.10 ML and 0.13 ML Au/MgO/Mo(100) indicates that non-metallic Au clusters do perturb the electronic structure of the  $\text{CH}_3\text{Br}$  molecule.

This work presents an example in which the evolution dynamics of the intermediate species of a photoinduced surface reaction are monitored in real time and correlated with the morphology and the electronic structure of the surface. Understanding the interplay between the elementary steps of surface reactions and surface properties could open new avenues to control surface photoinduced and photocatalytic chemical reactions through a rational design of the surface on which the reaction occurs.

## **Acknowledgements**

SRL gratefully acknowledge financial support provided by the U.S. Air Force Office of Scientific Research (Grant FA9550-19-1-0314). TMB acknowledges financial support provided by Deutsche Forschungsgemeinschaft and the Fonds der Chemischen Industrie as well as fruitful discussions with Christian Weigelt. TSR acknowledges financial support provided by the National Science Foundation (Grant NSF CHE-1955343). Density Functional Theory calculations were carried out on high-performance computer resources provided by STOKES, UCF Advanced Computing Center at University of Central Florida, and National Energy Scientific Computing Center (NERSC) at Lawrence Berkley National Laboratory.

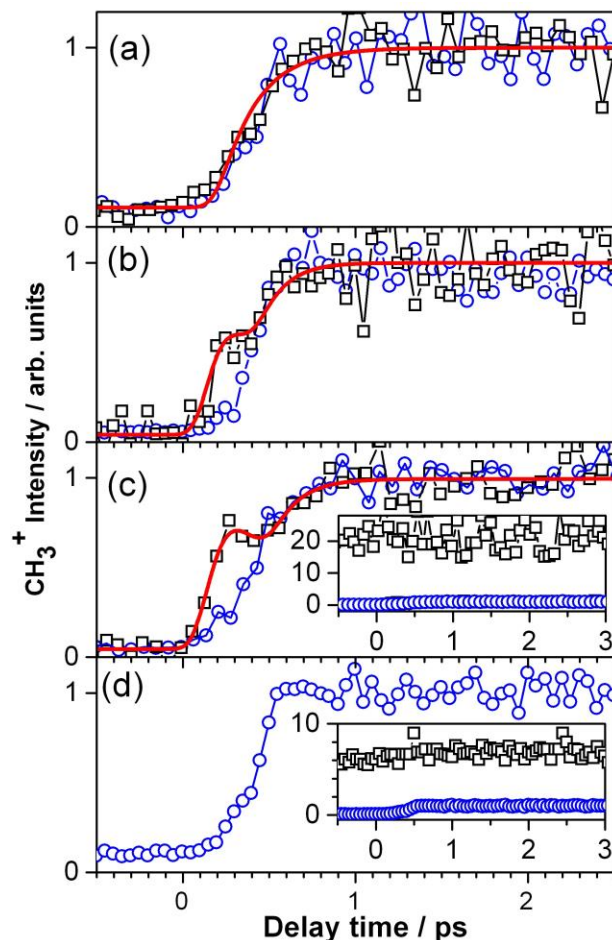
## References

1. *Gold Clusters, Colloids and Nanoparticles I*. Springer International Publishing: Cham, 2014.
2. *Gold Clusters, Colloids and Nanoparticles II*. Springer International Publishing: Cham, 2014.
3. Saha, K.; Agasti, S. S.; Kim, C.; Li, X.; Rotello, V. M., Gold Nanoparticles in Chemical and Biological Sensing. *Chem. Rev.* **2012**, *112* (5), 2739-2779.
4. Wang, Z.; Ma, L., Gold nanoparticle probes. *Coord. Chem. Rev.* **2009**, *253* (11), 1607-1618.
5. Das, M.; Shim, K. H.; An, S. S. A.; Yi, D. K., Review on gold nanoparticles and their applications. *Toxicol. Environ. Health Sci.* **2011**, *3* (4), 193-205.
6. Yeh, Y.-C.; Creran, B.; Rotello, V. M., Gold nanoparticles: preparation, properties, and applications in bionanotechnology. *Nanoscale* **2012**, *4* (6), 1871-1880.
7. Huang, X.; Jain, P. K.; El-Sayed, I. H.; El-Sayed, M. A., Gold nanoparticles: interesting optical properties and recent applications in cancer diagnostics and therapy. *Nanomedicine* **2007**, *2* (5), 681-693.
8. Notarianni, M.; Vernon, K.; Chou, A.; Aljada, M.; Liu, J.; Motta, N., Plasmonic effect of gold nanoparticles in organic solar cells. *Sol. Energy* **2014**, *106*, 23-37.
9. Lu, L.; Luo, Z.; Xu, T.; Yu, L., Cooperative Plasmonic Effect of Ag and Au Nanoparticles on Enhancing Performance of Polymer Solar Cells. *Nano Lett.* **2013**, *13* (1), 59-64.
10. Jun, H. K.; Careem, M. A.; Arof, A. K., Plasmonic Effects of Quantum Size Gold Nanoparticles on Dye-sensitized Solar Cell. *Mater. Today: Proc.* **2016**, *3*, S73-S79.
11. Liu, L.; Corma, A., Metal Catalysts for Heterogeneous Catalysis: From Single Atoms to Nanoclusters and Nanoparticles. *Chem. Rev.* **2018**, *118* (10), 4981-5079.
12. Munnik, P.; de Jongh, P. E.; de Jong, K. P., Recent Developments in the Synthesis of Supported Catalysts. *Chem. Rev.* **2015**, *115* (14), 6687-6718.
13. Stratakis, M.; Garcia, H., Catalysis by Supported Gold Nanoparticles: Beyond Aerobic Oxidative Processes. *Chem. Rev.* **2012**, *112* (8), 4469-4506.
14. Sarina, S.; Waclawik, E. R.; Zhu, H., Photocatalysis on supported gold and silver nanoparticles under ultraviolet and visible light irradiation. *Green Chem.* **2013**, *15* (7), 1814-1833.
15. Taylor, K. J.; Pettiette-Hall, C. L.; Cheshnovsky, O.; Smalley, R. E., Ultraviolet photoelectron spectra of coinage metal clusters. *J. Chem. Phys.* **1992**, *96* (4), 3319-3329.
16. Häkkinen, H.; Landman, U., Gold clusters Au<sub>N</sub> (2 ≤ N ≤ 10) and their anions. *Phys. Rev. B* **2000**, *62* (4), R2287-R2290.
17. Häkkinen, H.; Yoon, B.; Landman, U.; Li, X.; Zhai, H.-J.; Wang, L.-S., On the Electronic and Atomic Structures of Small Au<sub>N</sub><sup>-</sup> (N = 4–14) Clusters: A Photoelectron Spectroscopy and Density-Functional Study. *J. Phys. Chem. A* **2003**, *107* (32), 6168-6175.
18. Häkkinen, H.; Moseler, M.; Kostko, O.; Morgner, N.; Hoffmann, M. A.; v. Issendorff, B., Symmetry and Electronic Structure of Noble-Metal Nanoparticles and the Role of Relativity. *Phys. Rev. Lett.* **2004**, *93* (9), 093401.
19. Häkkinen, H.; Abbet, S.; Sanchez, A.; Heiz, U.; Landman, U., Structural, Electronic, and Impurity-Doping Effects in Nanoscale Chemistry: Supported Gold Nanoclusters<sup>13</sup>. *Angew. Chem. Int. Ed.* **2003**, *42*, 1297-1300.

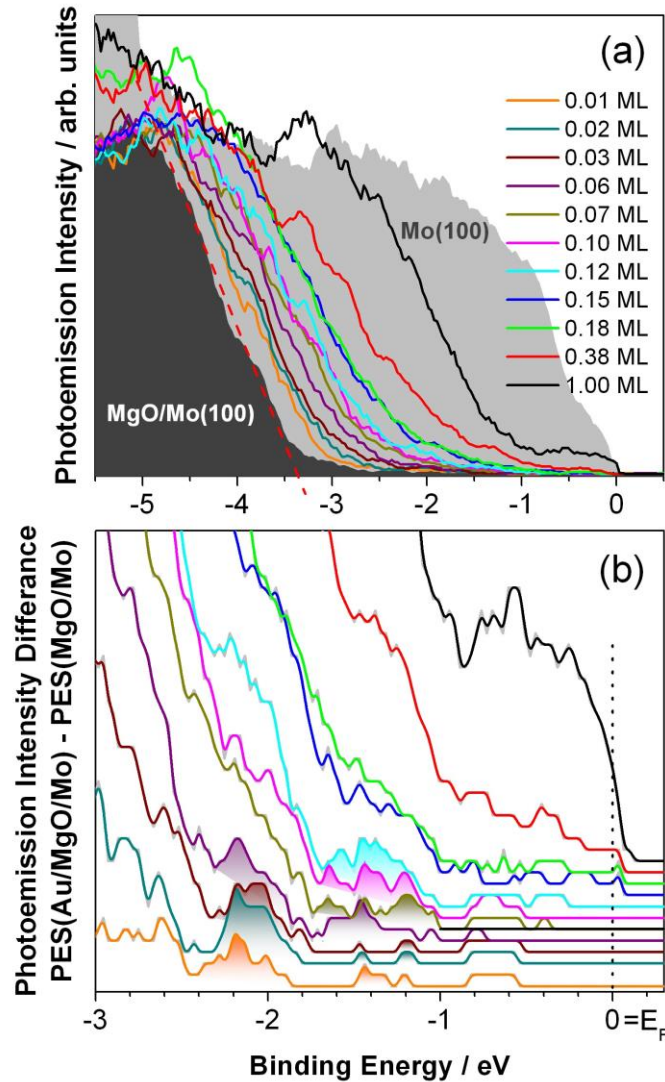
20. Furche, F.; Ahlrichs, R.; Weis, P.; Jacob, C.; Gilb, S.; Bierweiler, T.; Kappes, M. M., The structures of small gold cluster anions as determined by a combination of ion mobility measurements and density functional calculations. *J. Chem. Phys.* **2002**, *117* (15), 6982-6990.
21. Häkkinen, H.; Moseler, M.; Landman, U., Bonding in Cu, Ag, and Au Clusters: Relativistic Effects, Trends, and Surprises. *Phys. Rev. Lett.* **2002**, *89* (3), 033401.
22. Johansson, M. P.; Lechtken, A.; Schooss, D.; Kappes, M. M.; Furche, F., 2D-3D transition of gold cluster anions resolved. *Phys. Rev. A* **2008**, *77* (5), 053202.
23. Huang, W.; Wang, L.-S., Probing the 2D to 3D Structural Transition in Gold Cluster Anions Using Argon Tagging. *Phys. Rev. Lett.* **2009**, *102* (15), 153401.
24. Ferrighi, L.; Hammer, B.; Madsen, G. K. H., 2D–3D Transition for Cationic and Anionic Gold Clusters: A Kinetic Energy Density Functional Study. *J. Am. Chem. Soc.* **2009**, *131* (30), 10605-10609.
25. Mantina, M.; Valero, R.; Truhlar, D. G., Validation study of the ability of density functionals to predict the planar-to-three-dimensional structural transition in anionic gold clusters. *J. Chem. Phys.* **2009**, *131* (6), 064706.
26. Xiao, L.; Wang, L., From planar to three-dimensional structural transition in gold clusters and the spin–orbit coupling effect. *Chemical Physics Letters* **2004**, *392* (4), 452-455.
27. Li, J.; Li, X.; Zhai, H.-J.; Wang, L.-S., Au<sub>20</sub>: A Tetrahedral Cluster. *Science* **2003**, *299* (5608), 864-867.
28. Fernández, E. M.; Soler, J. M.; Garzón, I. L.; Balbás, L. C., Trends in the structure and bonding of noble metal clusters. *Phys. Rev. B* **2004**, *70* (16), 165403.
29. Zubarev, D. Y.; Boldyrev, A. I., Deciphering Chemical Bonding in Golden Cages. *J. Phys. Chem. A* **2009**, *113* (5), 866-868.
30. Yoon, B.; Koskinen, P.; Huber, B.; Kostko, O.; von Issendorff, B.; Häkkinen, H.; Moseler, M.; Landman, U., Size-Dependent Structural Evolution and Chemical Reactivity of Gold Clusters. *Chem. Phys. Chem.* **2007**, *8* (1), 157-161.
31. Gruene, P.; Rayner, D. M.; Redlich, B.; van der Meer, A. F. G.; Lyon, J. T.; Meijer, G.; Fielicke, A., Structures of Neutral Au<sub>7</sub>, Au<sub>19</sub>, and Au<sub>20</sub> Clusters in the Gas Phase. *Science* **2008**, *321* (5889), 674-676.
32. Bulusu, S.; Li, X.; Wang, L.-S.; Zeng, X. C., Evidence of hollow golden cages. *Proc. Natl. Acad. Sci.* **2006**, *103* (22), 8326-8330.
33. Sanchez, A.; Abbet, S.; Heiz, U.; Schneider, W. D.; Häkkinen, H.; Barnett, R. N.; Landman, U., When Gold Is Not Noble: Nanoscale Gold Catalysts. *J. Phys. Chem. A* **1999**, *103* (48), 9573-9578.
34. Heiz, U.; Schneider, W.-D., Nanoassembled model catalysts. *J. Phys. D: Appl. Phys.* **2000**, *33*, R85-R102.
35. Heiz, U.; Landman, U., *Nanocatalysis*. Springer-Verlag: Berlin, 2007.
36. Sanchez, A.; Abbet, S.; Heiz, U.; Schneider, W. D.; Hakkinen, H.; Barnett, R. N.; Landman, U., When Gold Is Not Noble: Nanoscale Gold Catalysts. *J. Phys. Chem. A* **1999**, *103*, 9573-9578.
37. Yamazoe, S.; Koyasu, K.; Tsukuda, T., Non-scalable Oxidation Catalysis of Gold Clusters. *Acc. Chem. Res.* **2014**, *47* (3), 816-824.
38. Landman, U.; Yoon, B.; Zhang, C.; Heiz, U.; Arenz, M., Factors in gold nanocatalysis: oxidation of CO in the non-scalable size regime. *Top. Catal.* **2007**, *44* (1), 145-158.
39. Huang, X.; El-Sayed, M. A., Gold nanoparticles: Optical properties and implementations in cancer diagnosis and photothermal therapy. *J. Adv. Res.* **2010**, *1* (1), 13-28.

40. Dykman, L. A.; Khlebtsov, N. G., Gold nanoparticles in chemo-, immuno-, and combined therapy: review. *Biomed. Opt. Express* **2019**, *10* (7), 3152-3182.
41. Vaida, M. E.; Bernhardt, T. M., Surface pump-probe femtosecond-laser mass spectrometry: Time-, mass-, and velocity-resolved detection of surface reaction dynamics. *Rev. Sci. Instrum.* **2010**, *81* (10), 104103-12.
42. Vaida, M. E.; Tchitnga, R.; Bernhardt, T. M., Femtosecond time-resolved photodissociation dynamics of methyl halide molecules on ultrathin gold films. *Beilstein J. Nanotechnol.* **2011**, *2*, 618-627.
43. Vaida, M. E.; Bernhardt, T. M., Surface-aligned femtochemistry: Photoinduced reaction dynamics of CH<sub>3</sub>I and CH<sub>3</sub>Br on MgO(100). *Faraday Discuss.* **2012**, *157*, 437-449.
44. Vaida, M. E.; Gleitsmann, T.; Tchitnga, R.; Bernhardt, T. M., Femtosecond-laser photoemission and photodesorption from magnesia supported gold clusters. *Phys. Status Solidi B* **2010**, *247* (5), 1139-1146.
45. Vaida, M. E.; Bernhardt, T. M., Surface-aligned femtochemistry: Molecular reaction dynamics on oxide surfaces. In *Springer Series in Chemical Physics 107*, Nalda, R. d.; Bañares, L., Eds. Springer Verlag: 2014.
46. Vaida, M. E.; Bernhardt, T. M., Tuning the ultrafast photodissociation dynamics of CH<sub>3</sub>Br on ultrathin MgO films by reducing the layer thickness to the 2D limit. *Chem. Phys. Lett.* **2017**, *688*, 106-111.
47. Vaida, M. E.; Leone, S. R., Tracing dissociation dynamics of CH<sub>3</sub>Br in the 3Q0 state with femtosecond extreme ultraviolet ionization. *Chem. Phys.* **2014**, *442*, 41-47.
48. Vaida, M. E.; Hindelang, P. E.; Bernhardt, T. M., Femtosecond real-time probing of transition state dynamics in a surface photoreaction: Methyl desorption from CH<sub>3</sub>I on MgO(100). *J. Chem. Phys.* **2008**, *129*, 011105.
49. Sterrer, M.; Risse, T.; Heyde, M.; Rust, H.-P.; Freund, H.-J., Crossover from Three-Dimensional to Two-Dimensional Geometries of Au Nanostructures on Thin MgO(001) Films: A Confirmation of Theoretical Predictions. *Phys. Rev. Lett.* **2007**, *98*, 206103.
50. Yulikov, M.; Sterrer, M.; Risse, T.; Freund, H. J., Gold atoms and clusters on MgO(100) films; an EPR and IRAS study. *Surf. Sci.* **2009**, *603* (10-12), 1622-1628.
51. Popolan, D. M.; Bernhardt, T. M., Interaction of gold and silver cluster cations with CH<sub>3</sub>Br: thermal and photoinduced reaction pathways. *Eur. Phys. J. D* **2011**, *63* (2), 251-254.
52. White, X.-L. Z. a. J. M., Alkyl halide photochemistry on Ag(111). *Surf. Sci.* **1991**, *241*, 270-278.
53. Vaida, M. E.; Marsh, B. M.; Leone, S. R., Nonmetal to Metal Transition and Ultrafast Charge Carrier Dynamics of Zn Clusters on p-Si(100) by fs-XUV Photoemission Spectroscopy. *Nano Lett.* **2018**, *18* (7), 4107-4114.
54. Marsh, B. M.; Vaida, M. E.; Cushing, S. K.; Lamoureux, B. R.; Leone, S. R., Measuring the Surface Photovoltage of a Schottky Barrier under Intense Light Conditions: Zn/p-Si(100) by Laser Time-Resolved Extreme Ultraviolet Photoelectron Spectroscopy. *J. Phys. Chem. C* **2017**, *121* (40), 21904-21912.
55. Vaida, M. E.; Leone, S. R., Femtosecond Extreme Ultraviolet Photoemission Spectroscopy: Observation of Ultrafast Charge Transfer at the n-TiO<sub>2</sub>/p-Si(100) Interface with Controlled TiO<sub>2</sub> Oxygen Vacancies. *J. Phys. Chem. C* **2016**, *120* (5), 2769-2776.
56. Perego, M.; Seguni, G.; Scarel, G.; Fanciulli, M.; Wallrapp, F., Energy band alignment at TiO<sub>2</sub>/Si interface with various interlayers. *J. Appl. Phys.* **2008**, *103* (4), 043509-1 - 043509-6.

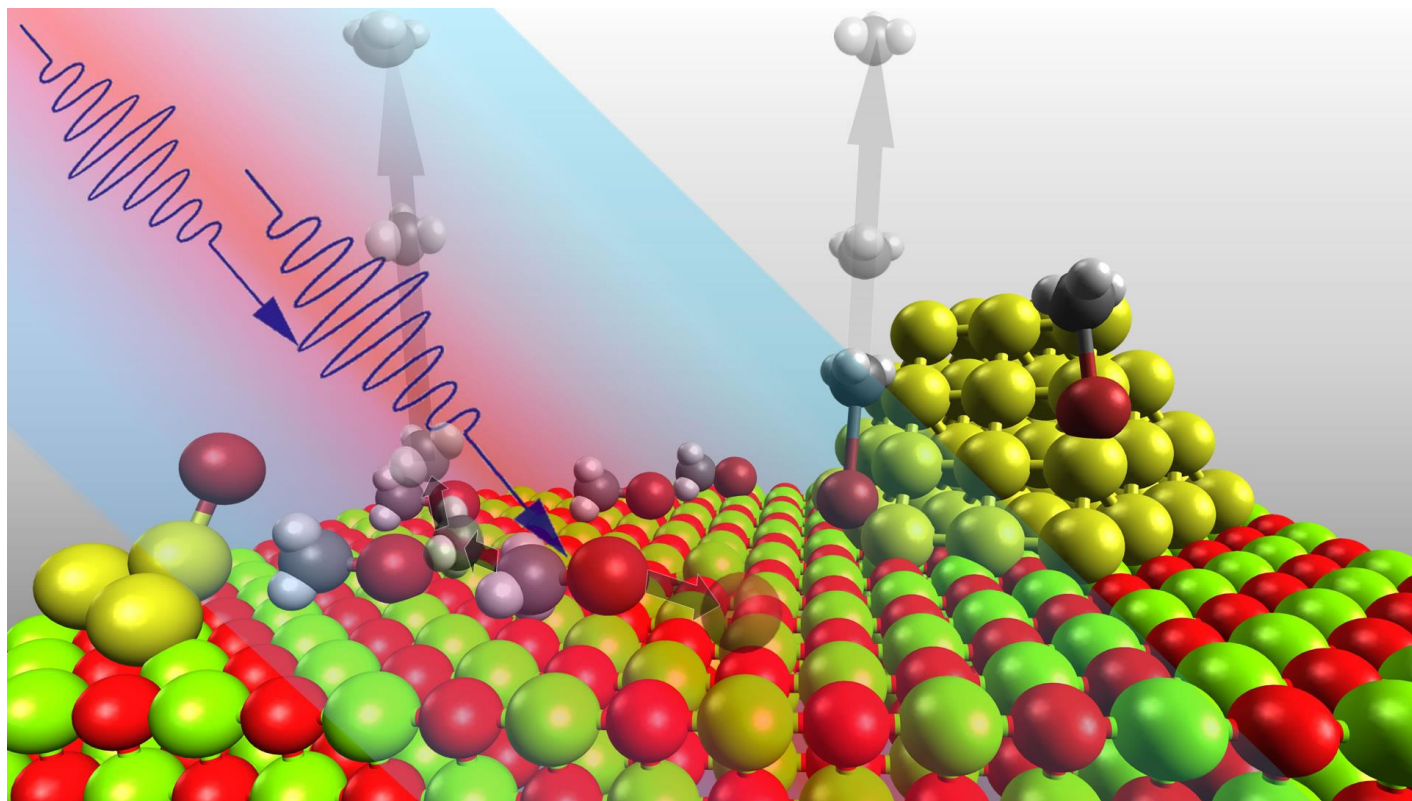
57. Ricci, D.; Bongiorno, A.; Pacchioni, G.; Landman, U., Bonding Trends and Dimensionality Crossover of Gold Nanoclusters on Metal-Supported MgO Thin Films. *Phys. Rev. Lett.* **2006**, *97*, 036106-4.
58. Giordano, L.; Baistrocchi, M.; Pacchioni, G., Bonding of Pd, Ag, and Au atoms on MgO(100) surfaces and MgO/Mo (100) ultra-thin films: A comparative DFT study. *Phys. Rev. B* **2005**, *72*, 115403.
59. Honkala, K.; Hakkinen, H., Au Adsorption on Regular and Defected Thin MgO(100) Films Supported by Mo. *J. Phys. Chem. C* **2007**, *111*, 4319.



**Figure 1.** Femtosecond time-resolved pump-probe mass signals of methyl cations detected after photodissociation of  $\text{CH}_3\text{Br}$  adsorbed on the bare  $\text{MgO}/\text{Mo}(100)$  substrate (blue circles) and from  $\text{CH}_3\text{Br}$  adsorbed on the same  $\text{MgO}/\text{Mo}(100)$  surface covered by gold particles (black squares). The transient signals are normalized to the highest intensity. The gold coverages are (a) 0.065 ML Au; (b) 0.10 ML Au; (c) 0.13 ML Au; (d) 0.15 ML Au. The transient signals were obtained with  $6 \text{ mW}/\text{cm}^2$  pump (266 nm) and  $600 \text{ mW}/\text{cm}^2$  probe laser power (333 nm). The red curves are the best fit of a ‘delayed exponential rise’ model in panel (a) and a ‘peak’ in conjunction with a ‘delayed exponential rise’ model to the experimental data in panels (b) and (c). The inset in (c) displays the relative intensity of the  $\text{CH}_3^+$  signal recorded from a magnesia film covered with 0.13 ML Au that was briefly annealed at 800 K (black squares) together with the  $\text{CH}_3^+$  transient signal recorded from the bare magnesia surface (blue circles). The inset in panel (d) shows the relative intensity of the  $\text{CH}_3^+$  signal recorded before (blue circles) and after covering a magnesia film with 0.15 ML Au (black squares). All pump-probe experiments, Au deposition, and  $\text{CH}_3\text{Br}$  dosage are performed at a surface temperature of 100 K.



**Figure 2.** (a) Photoemission spectra recorded from various amounts of Au evaporated on 10 ML MgO(100)/Mo(100) at 100 K. The light grey and dark grey filled curves are the measured photoemission spectra of bare Mo(100) and of 10 ML MgO grown on Mo(100), respectively. The legend shows the Au coverage in monolayer equivalent. The dashed line represents the linear extrapolation of the O-2p rising edge used for the determination of the valence band maximum of the MgO(100) thin film. All photoemission spectra were recorded with the 23<sup>rd</sup> harmonic (35.65 eV) of the fundamental wavelength of Ti:Sapphire femtosecond laser. (b) Difference between the photoemission spectra obtained from Au/MgO/Mo(100) and the photoemission spectrum obtained from MgO/Mo(100). The vertical dashed line indicates the Fermi level. Colored curves in (b) are smoothed spline interpolations of the raw data points plotted in light gray.



Graphical abstract